



OPEN

Characterization of non-linear mechanical behavior of the cornea

A. Ashofteh Yazdi^{1,2}, J. Melchor^{3,4,5}, J. Torres^{1,4}, I. Faris^{1,4}, A. Callejas^{1,4}, M. Gonzalez-Andrades^{6,7}✉ & G. Rus^{1,4,5}✉

The objective of this study was to evaluate which hyperelastic model could best describe the non-linear mechanical behavior of the cornea, in order to characterize the capability of the non-linear model parameters to discriminate structural changes in a damaged cornea. Porcine corneas were used, establishing two different groups: control (non-treated) and NaOH-treated (damaged) corneas (n = 8). NaOH causes a chemical burn to the corneal tissue, simulating a disease associated to structural damage of the stromal layer. Quasi-static uniaxial tensile tests were performed in nasal-temporal direction immediately after preparing corneal strips from the two groups. Three non-linear hyperelastic models (i.e. Hamilton-Zabolotskaya model, Ogden model and Mooney-Rivlin model) were fitted to the stress–strain curves obtained in the tensile tests and statistically compared. The corneas from the two groups showed a non-linear mechanical behavior that was best described by the Hamilton-Zabolotskaya model, obtaining the highest coefficient of determination ($R^2 > 0.95$). Moreover, Hamilton-Zabolotskaya model showed the highest discriminative capability of the non-linear model parameter (Parameter A) for the tissue structural changes between the two sample groups ($p = 0.0005$). The present work determines the best hyperelastic model with the highest discriminative capability in description of the non-linear mechanical behavior of the cornea.

The cornea is the outermost layer of the eye, acting as a barrier against the external environment and as the main diopter of the visual system¹. Diseases that affect the cornea are one of the main causes of blindness in the world, ranking among the three most prevalent worldwide². Among those, corneal ectasia or corneal ectatic disorders stand as a main priority because of their incidence and impact in young population. These are corneal disorders, such as keratoconus or pellucid marginal corneal degeneration, that cause alterations in the corneal structure, leading to corneal topographical changes with decreased corneal thickness and abnormal corneal curvature³. This abnormal structure of the cornea, as a result of non-linear mechanical changes, finally causes visual impairment to the patient. Currently, the diagnose of corneal degenerations and other corneal diseases are mainly based on structural measurements of the cornea (i.e. curvature, thickness, etc.), while some studies covered in-vivo non-structural measurements using Oculus Corvis ST and Ocular Response Analyzer systems^{4–6}. These new, non-invasive systems can analyze corneal biomechanical properties, such as corneal hysteresis, including an estimation of intraocular pressure. However, we propose that non-linear mechanical parameters can be obtained from non-invasive elastography or probing technologies such as non-linear torsional waves, non-linearity in probing, non-linearity by micro-indentation to be used in diagnostics in-vivo without removing the cornea^{7–9}. Hence, quantifying the non-linear mechanical parameters of soft tissues like the cornea might become more specific diagnostic criteria than structural measurements. This is supported by the fact that non-linear mechanical characterization and non-linear model parameters are very sensitive realistic approaches to measure the tissue structural damages^{7,8}. The feasibility of early diagnosis of corneal diseases such as keratoconus is however an open issue to be investigated in the future. This will depend on the precision of the nonlinearity parameter achievable by the selected probing technology, and thereof define the sensitivity and sensibility. Despite of that, non-linear

¹Ultrasonics Lab, Department of Structural Mechanics, University of Granada, Politécnico de Fuentenuueva, 18071 Granada, Spain. ²Department of Biomedical Engineering, Islamic Azad University, Mashhad Branch, Mashhad, Iran. ³Department of Statistics and Operations Research, University of Granada, Granada, Spain. ⁴Instituto de Investigación Biosanitaria, Ibs.GRANADA, Granada, Spain. ⁵Excellence Research Unit, "Modelling Nature" (MNat), University of Granada, Granada, Spain. ⁶Maimonides Biomedical Research Institute of Cordoba (IMIBIC), Department of Ophthalmology, Reina Sofia University Hospital and University of Cordoba, Edificio IMIBIC, Av. Menéndez Pidal, s/n. 14004, Cordoba, Spain. ⁷Massachusetts Eye and Ear and Schepens Eye Research Institute, Department of Ophthalmology, Harvard Medical School, Boston, MA, USA. ✉email: miguel.gonzalez@imibic.org; grus@ugr.es

elastic constants may be much more sensitive to specific diseases, i.e. expressing larger variations than linear ones, which might facilitate an early diagnosis⁹.

Thus, non-linear models might facilitate to understand how corneal diseases affect the structure and the mechanical behavior of the cornea, and how this leads to blurred vision, or even blindness, in combination with other strategies. In order to determine the direct effect on vision, these models should be combined with methods to calculate the changes in geometry and methods to trace the light through the optical system or wave-front calculations^{10–12}. Moreover, non-linear models could improve the diagnosis of some corneal diseases such as keratoconus, in addition to facilitate the evaluation of specific therapeutic strategies like corneal collagen crosslinking¹³. To achieve this, measurements of the elastic or shear modulus in healthy and abnormal corneas are required. Many studies have measured the elastic modulus of healthy and keratoconus corneas using uniaxial tensile tests or high-resolution ultrasound techniques^{14–18}. Several studies showed that keratoconus cornea stands in contrast to the healthy cornea, both in regard to mechanics and collagen structure^{19,20}. Specifically, it has been proposed that collagen structure varies axially in keratoconus cornea compared to the healthy cornea^{21,22}. As the collagen structure is directly tied to the biomechanical properties, it is expected that mechanical properties will vary in the axial direction²³.

Numerical models are intended to contribute to future *in-vivo* biomechanical analysis. There have been a significant number of studies which have developed the constitutive models of the non-linear viscoelastic behavior of soft tissues. Hamilton-Zabolotskaya separated the effects of compressibility and shear deformation by expanding a fourth-order isotropic elastic energy density introduced by Landau and Lifshitz^{24,25}. Destrade et al. (2010) demonstrated that the third-order behavior of incompressible solids with parallel fibers can be described by 7 elastic constants²⁶. Ye et al. (2018) introduced a finite element formulation to show the non-linear behavior of finite amplitude shear waves in soft solids, considering a visco-hyperelastic Landau's model²⁷.

Some other models were developed to describe the mechanical behavior of cornea in quasi-static and dynamic states. Alastrué et al. (2005) considered a nonlinear anisotropic hyperelastic behavior model of the cornea that strongly depends on the physiological collagen fibril distribution under a finite element context²⁸. Pandolfi and Holzapfel (2008) proposed a three-dimensional computational model for the human cornea that was able to provide the refractive power by analyzing the structural mechanical response with the non-linear regime and the effect of the intraocular pressure²⁹. Elsheikh et al. (2010) employed non-linear finite element analysis of corneal models to assess the importance of considering the cornea's hyperelastic, hysteretic and anisotropic behavior, multi-layer construction, weak inter-lamellar adhesion, non-uniform thickness, elliptical topography, and connection to the sclera³⁰. Nguyen et al. (2010) developed an inverse finite element method to determine the anisotropic properties of bovine cornea from an *in-vitro* inflation experiment³¹. Su et al. (2014) derived a corneal hyper-viscoelastic model to describe the material properties more accurately, and explained the mathematical method for determination of the model parameters³². Whitford et al. (2017) introduced the combination of the complex anisotropic representation, shear stiffness and regional variation of fibril density of the human cornea with its viscoelastic behavior. The study further attempted to calibrate the proposed model with existing *ex-vivo* human data³³.

Despite of the capability to describe part of the mechanical behavior of the cornea, none of these models can fit the non-linear corneal mechanical behavior with $R^2 > 0.9$, lacking discriminative parameters for the description of structural changes under non-linear models with $P < 0.05$. Therefore, there is a critical need to find a model that can highly fit to the non-linear mechanical behavior of the cornea. The objective of this study was to evaluate which non-linear model could best describe the mechanical behavior of the corneal tissues, including the characterization of the discriminative capability of the model to distinguish the structural changes between the healthy and damaged corneas. To this purpose, three hyperelastic models (i.e. Hamilton-Zabolotskaya, Ogden and Mooney-Rivlin models) were fitted to the stress-strain results from healthy and NaOH-treated corneas in order to obtain the non-linear model parameters.

Materials and methods

Sample preparation. Due to the limitations of human corneal tissue sampling, porcine models have been widely used for understanding physiological changes of the healthy and damaged tissue. The similarity of structural components of porcine samples to the human ones, results in a good insight to the mechanical behavior of the cornea³⁴. The porcine eye globes were taken immediately post-mortem from a local slaughter house. The eyes were kept in a lab freezer at $-20\text{ }^\circ\text{C}$ to avoid tissue degradation until being prepared for the tests. The samples were excised from the eye globe with 2 mm of sclera. Two different groups were prepared ($n = 8$): control (non-treated) and NaOH-treated (damaged) groups (Fig. 1). For the NaOH-treated group, corneal buttons were soaked in 1.5 M NaOH for 2 min, followed by washing using water and phosphate buffer saline (PBS) each for 2 min, independently. Alkali solution causes a chemical burn to the corneal tissue, simulating a disease associated to structural damage of the stromal layer³⁵. Afterwards, tissue strips were prepared by a custom made bladed punch. All the tissue strips were only excised in temporal-nasal direction in order to avoid anisotropic variations of mechanical properties.

Uniaxial tensile tests. The stress-strain behavior of the two groups of corneal tissues was measured by using a custom made uniaxial tensile machine (Fig. 2a). The uniaxial tensile machine was designed, fabricated and calibrated for the mechanical characterization of soft tissues at the Ultrasonics Lab, University of Granada, Spain. Force was measured using an Imada ZTA-500 force measurement system, connected to a PC by USB and an automated Matlab code to record and analyze the force results with an accuracy of $\pm 0.2\%$, and displacement was obtained through the movement of the uniaxial tensile stepper motors at each increment with precision less than 5 microns (Fig. 2b). The displacement was measured by averaging the deformation of the complete probe,

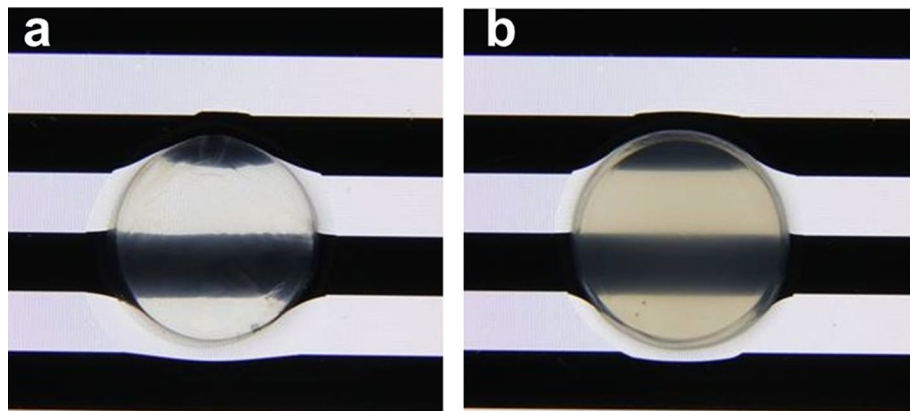


Figure 1. Representative pictures of the non-treated (a) and NaOH-treated (b) corneas, after obtaining the central corneal button by trephination. Corneal buttons were placed on a standardized black and white band illuminated pattern in order to show the changes on transparency after the alkali burn.

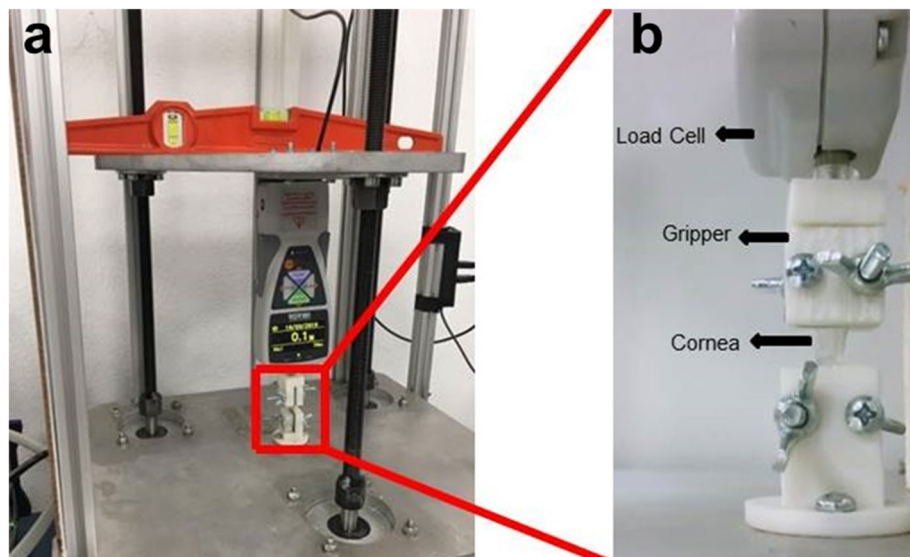


Figure 2. The front view of the uniaxial tensile setup (a) and its lateral (camera) view (b).

Groups	Ave. length (mm)	Ave. width (mm)	Ave. central thickness (mm)
Control group	16.02 ± 1.33	5.24 ± 1.67	1.56 ± 0.22
NaOH-treated group	13.12 ± 2.45	5.05 ± 0.97	1.76 ± 0.21
P-value	0.16	0.789	0.1

Table 1. The average measured dimensions of the samples in different groups.

while the reality is that the deformation will concentrate on the narrow part of the probe. Therefore, the limitation is that the clamps and the parts of the specimen close to the clamps were neglected, which implies a bias (non-random error), which should not alter the hypothesis testing purposes, as they affect like a proportional constant across all the tests, and therefore is canceled-out at the hypothesis testing. A high resolution camera, IPEVO Ziggi-HD High Definition USB CDVU-04IP model 5MPix 4:3 ratio 2,560 × 1,920, was used to monitor the tissue deformation but not to measure displacements. The uniaxial tensile tests were performed immediately after preparing the corneal strips from the two groups in order to avoid changes in the mechanical response of the tissue.

Prior to the experiments, the length, width and thickness of the corneal strips were measured using a digital caliper (Table 1). No significant differences were found between the groups, while the samples length–width

ratio was not enough low to be concerned about clamping issues³⁶. The samples were pre-conditioned at a low strain regime, namely 5%, to gain the mechanical response of the corneal tissue close to in-vivo conditions³⁷. The tissues underwent a quasi-static uniaxial tensile displacement to the rupture point at a rate of 0.2 mm/s. This testing technique is unable to represent the in-vivo condition. However, it is suitable for finding which hyperelastic model could best describe the non-linear mechanical behavior of the cornea. No significant dehydration of the samples was observed during the tests. The tensile stress and strain were calculated by dividing the measured force, maximally 24.6 N and 15 N for the control and damaged samples respectively, by the initial cross-sectional area and the displacement by the initial length of the strips, respectively^{38,39}. The thickness of the samples was considered constant during the test.

Mechanical analysis. The tensile stress and strain were calculated using the force and displacement measured in the tests as functions of time. Curve fitting tool in MATLAB R2018a, using the non-linear least squares method, was implemented to fit best non-linear models to the stress–strain curves. The material parameters were adjusted by defining ranges of values, according to the literature, in order not to obtain negative or non-realistic parametric values, while the least squares method is the algorithm that solves the inverse problem of fitting a hyperelastic model to the experimental data by minimizing a residue⁴⁰.

The elastic response of the tissues was described by the three hyperelastic models: Hamilton-Zabolotskaya model, Ogden model and Mooney-Rivlin model (Eqs. 1, 2 and 3, respectively)^{24,41,42}.

$$E = \mu \cdot I_2 + (1/3) \cdot A \cdot I_3 + D \cdot I_2^2 \quad (1)$$

$$f = \sigma \cdot \lambda^{-1} = \mu \cdot ((\lambda^{\alpha-1}) - (\lambda^{-(1+0.5\alpha)})) \quad (2)$$

$$\sigma = 2 \cdot (\lambda^2 - 1/\lambda) \cdot (C_1 + C_2 \cdot 1/\lambda) \quad (3)$$

where in Eq. (1), E is a strain energy function; coefficient μ is the shear modulus, parameters A and D indicate the third and fourth order elastic constants of the stress–strain curves and I_2 and I_3 are the second and third order lagrangian strain invariants.

In Eq. (2), λ indicates the stretch ratio, μ and α are the shear modulus coefficients.

Where in Eq. (3), λ , C_1 and C_2 indicate the stretch ratio and the Mooney–Rivlin material constants, respectively.

Statistical analysis. A coefficient of determination R^2 was considered for the acceptance of the models fitted to the experimental results. The minimum $R^2=0.9$ was considered for the acceptance of the hyperelastic models fitted to the two sample groups^{38,39}. Two samples T-test, using MATLAB R2018a function `ttest2`, was implemented to study the significance of the non-linear model parameters, as well as dimensions of samples, for the structural changes between the two sample groups. A value of $p < 0.05$ was considered statistically significant for the differences of the non-linear parameters between the control and NaOH-treated groups. n.s., *, **, ***, and **** represent p greater than 0.05, $p < 0.05$, $p < 0.01$, $p < 0.001$ and $p < 0.0001$, respectively. The estimated coefficients were represented graphically with box plots. Additionally, the Pearson correlation coefficients for the model parameters between the two groups were calculated.

Results

The uniaxial tensile tests were performed to the rupture point on the two groups of 8 corneal samples, control and NaOH-treated, as shown in Fig. 3a. The strain data were acquired immediately before the initial resistance from the tissue was observed. Fitting the non-linear models requires estimating all the parameters including linear modulus, where it is an important parameter to be explored in order to validate the results. A significant difference was observed in the elastic modulus, which was defined as the slope of the tangent to the stress–strain curves at the initial stage of elastic region, between the two groups ($p=0.0005$) (Fig. 3b), as well as the tensile strength ($p=0.0005$) (Fig. 3c).

The coefficient of determination R^2 of the three hyperelastic models fitted to the elastic response of the two groups (Fig. 4). A minimum R^2 of 0.9 was considered for the acceptance of the best models fitted.

For the Hamilton-Zabolotskaya model, the difference between the third order elastic constant (parameter A) for the two groups was found to be significant ($p=0.0005$) (Fig. 5a). The difference between the fourth order elastic constant (parameter D) for the two groups was significant, as well ($p=0.0045$) (Fig. 5b).

For the Ogden model, the coefficient μ was found to be significantly different for the two groups ($p=0.017$) (Fig. 6a). The coefficient α was different between the two groups ($p=0.055$) (Fig. 6b).

For the Mooney-Rivlin model, the material constants C_1 and C_2 were significantly different for the two groups, ($p=0.001$) and ($p=0.002$), respectively (Fig. 7).

The mean and standard deviation of the non-linear parameters of the three hyperelastic models for the two groups are shown in Table 2.

The Pearson correlation coefficients between the two groups were calculated for each parameter of the three hyperelastic models (Table 3).

In addition, the Pearson correlation coefficients between the model parameters of each hyperelastic model were calculated (Table 4).

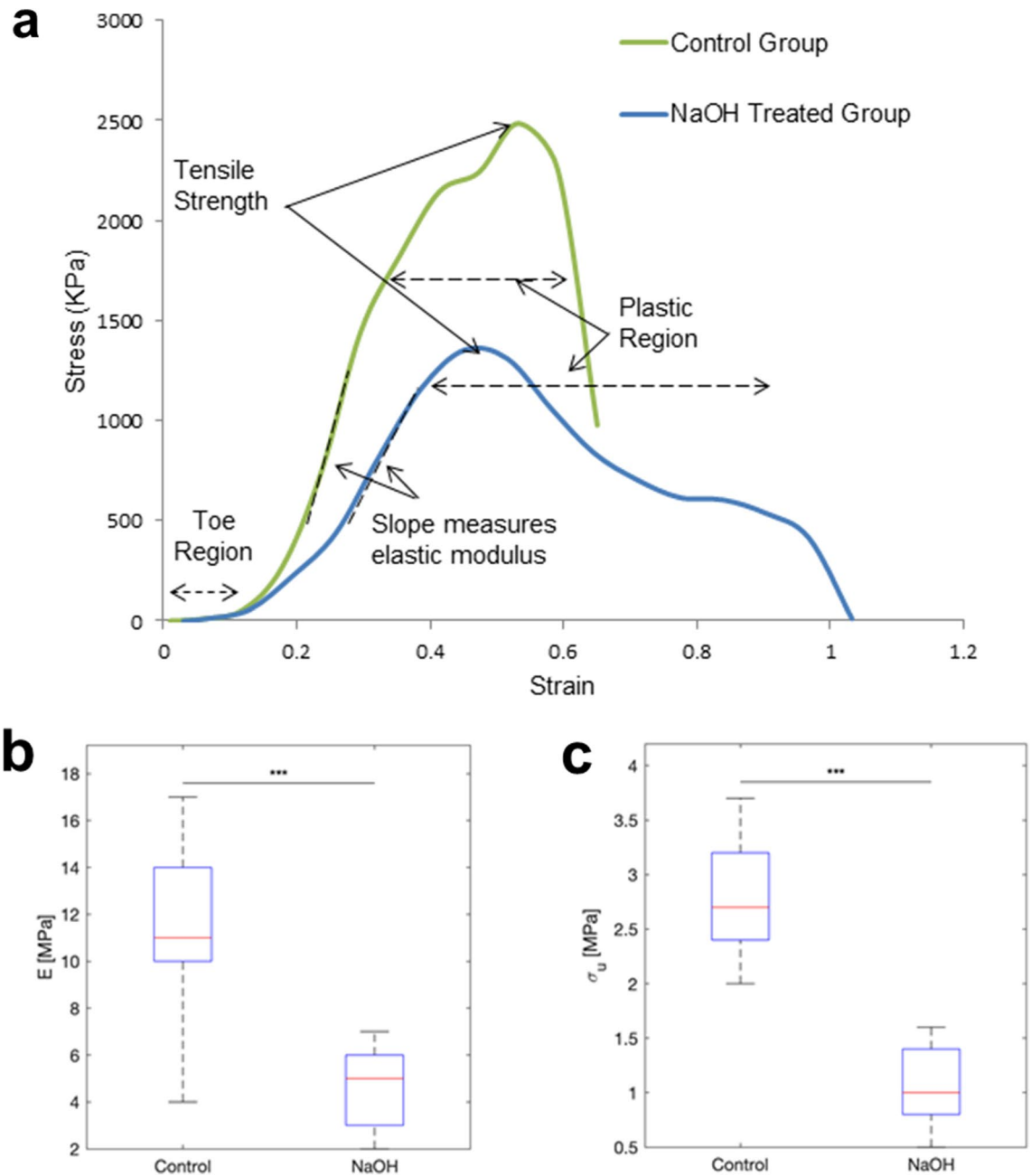


Figure 3. Representative stress–strain curves for the two groups (control versus NaOH-treated group) (a). Elastic modulus (b) and tensile strength (c) were significantly different between the groups ($p = 0.0005$).

Discussion

Quantifying the non-linear mechanical parameters of soft tissues has the potential to become specific diagnostic criteria for some corneal diseases, due to the fact that non-linear mechanical characterization and non-linear model parameters are very sensitive realistic approaches to measure the tissue structural damages, i.e. expressing larger variations than linear ones. In tensile testing, the non-linear behavior is apparent at high strains, but there are emerging elastography and probing technologies that precisely quantify non-linearity at extremely low strains. For instance, harmonic generation technique measures the amplitude of the harmonics when tissue is excited with ultrasound at strains of the order of 10^{-5} , and these harmonic amplitudes are proportional to the non-linearity^{43–45}. There have been a significant number of studies which have improved the non-linear models of corneal tissue biomechanics. Nevertheless, this was the first work to describe the non-linear mechanical behavior of the corneal tissue including the characterization of the discriminative capability of the model to distinguish structural changes between the healthy and damaged cornea.

Hyperelastic models are suitable for characterization of non-linear mechanical behavior of soft tissues involving large deformations. Hyperelastic constitutive laws are used to model materials that respond elastically when subjected to very large strains. They account both for nonlinear material behavior and large shape changes⁴⁶.

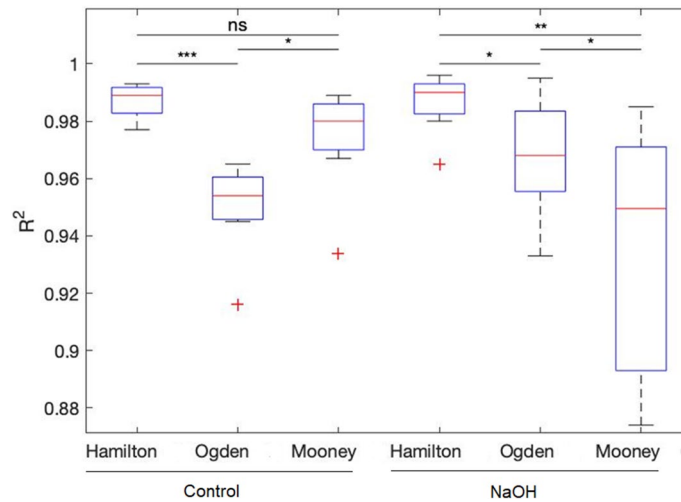


Figure 4. The coefficient of determination R^2 of the three hyperelastic models fitted to the elastic response of the control and NaOH-treated groups.

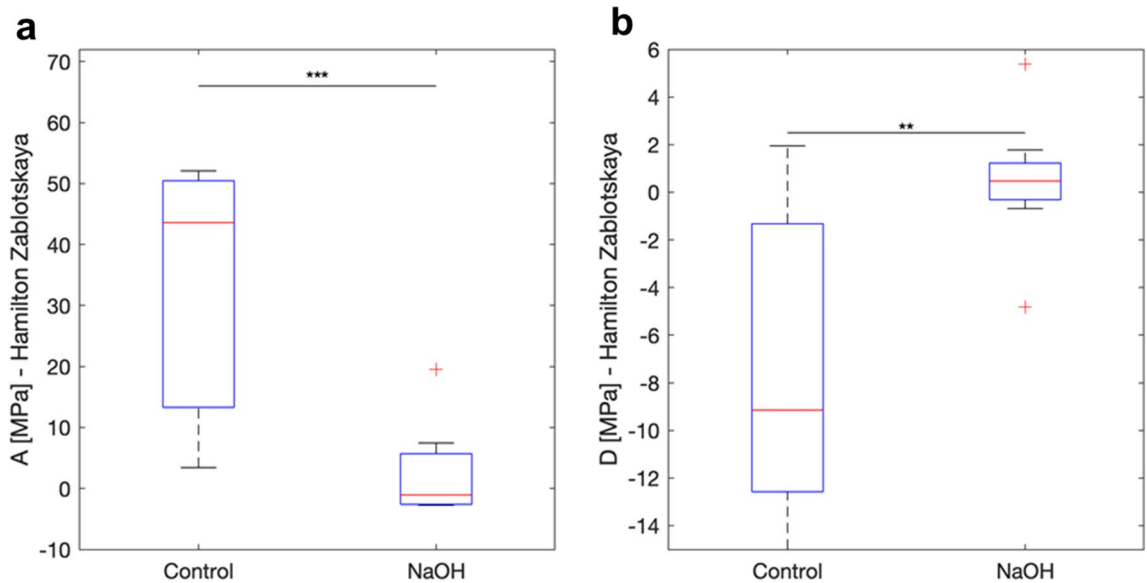


Figure 5. Hamilton–Zabolotskaya model. The parameter A was significantly different between the two groups ($p=0.0005$) (a). The parameter D difference between the two groups was significant ($p=0.0045$) (b).

The non-linear elastic response of the corneal tissue was well described by the three hyperelastic models: Hamilton–Zabolotskaya model, Ogden model and Mooney–Rivlin model. The Hamilton–Zabolotskaya model was best fitted to the stress–strain results for the two sample groups with the highest coefficient of determination R^2 . It was proved that the third and fourth order elastic constants could best characterize the non-linear mechanical behavior of the control and damaged corneal tissues.

The Hamilton–Zabolotskaya model constants were measured and compared for the two sample groups. A significant difference in the third and fourth order elastic constants (parameters A and D) between the two sample groups, $p=0.0005$ and $p=0.0045$, respectively, was in accordance with previous results related to corneal stromal damage^{14,23}. This resulted in a significant decrease in the tensile strength of the tissue. A negative correlation coefficient was found for parameters A and D between the two sample groups, indicating the differences in the structural behavior of control corneas versus NaOH-treated ones. This suggests that the damage caused to the stromal layer after treating with NaOH led to alterations in the collagen architecture, showing similar mechanical effects to those observed in keratoconus^{14,23}.

The Ogden model showed a significant difference in the coefficient μ between the two sample groups, ($p=0.017$), which could be related to different facts. Specifically, the shear strength was considerably decreased for the NaOH-treated samples possibly due to the disorganization of the tissue structure^{14,23}. The coefficient α increased for the NaOH-treated samples ($p=0.055$), indicating a loss in the shear stiffness of the tissues. This

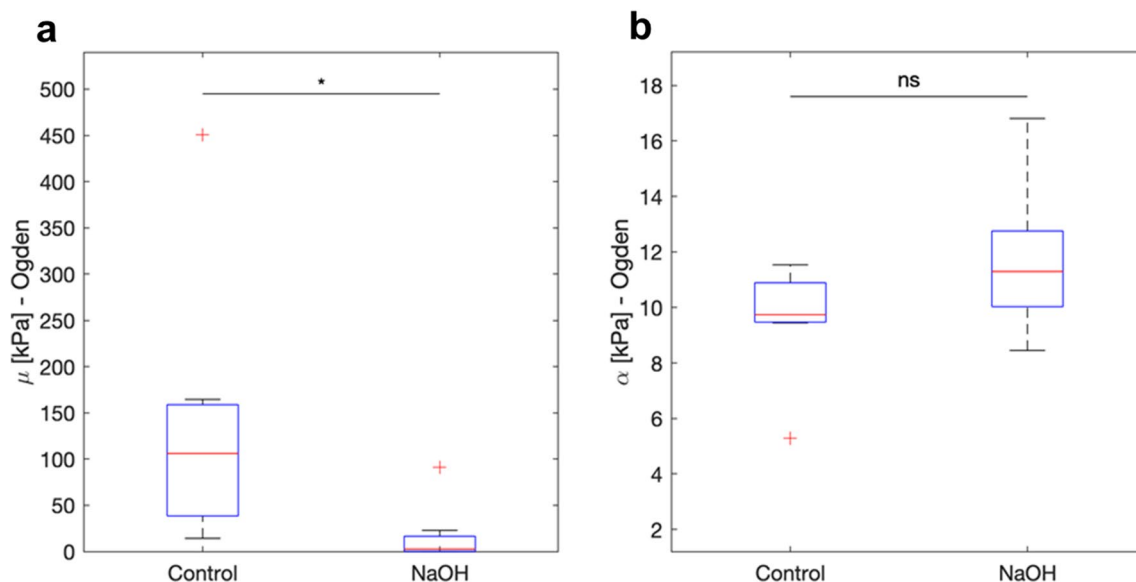


Figure 6. Ogden model. The coefficient Mu (μ) was significantly different for the two groups ($p=0.017$) (a). The coefficient Alpha (α) was different but not significant for the two groups ($p=0.055$) (b).

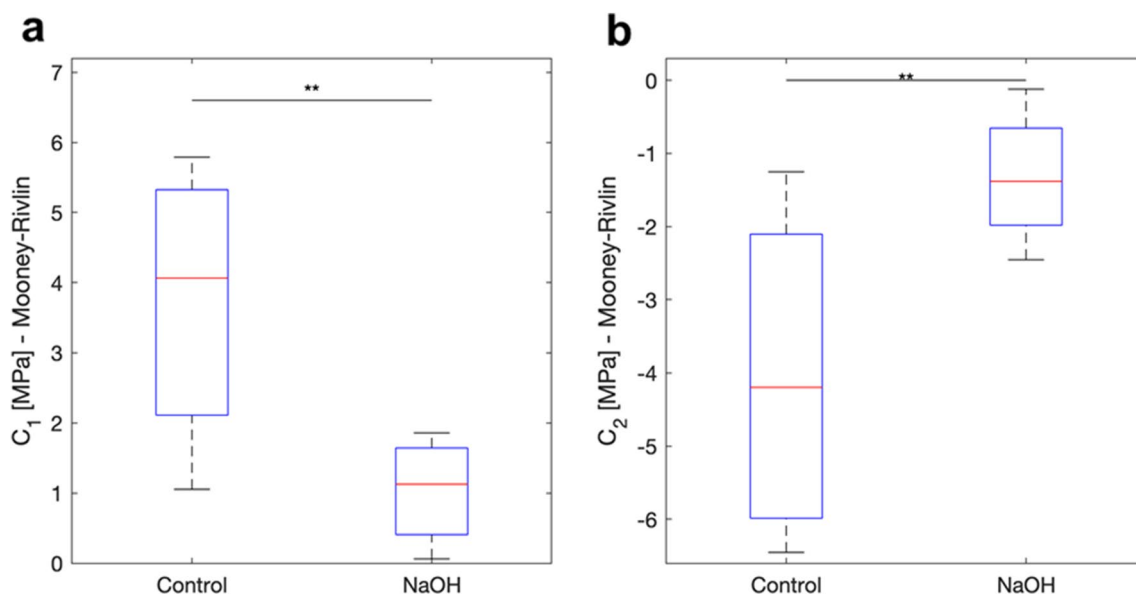


Figure 7. Mooney-Rivlin model. The coefficient C1 was significantly different for the two groups ($p=0.001$) (a). The coefficient C2 was also significantly different for the two groups ($p=0.002$) (b).

Non-linear parameters	Parameter A	Parameter D	Coefficient μ	Coefficient α	Constant C_1	Constant C_2
Control group	34,153.42 ± 20,918.87	-7,796.18 ± 6,974.51	142.36 ± 147.47	9.58 ± 2.04	3,706 ± 1816.18	-4,122.42 ± 2,102.4
NaOH-treated group	1,054.52 ± 9,926.87	416.87 ± 2,811.81	16.24 ± 31.27	11.67 ± 2.59	1,034.24 ± 686.98	-1,327.61 ± 287.44
P-value	0.0005	0.0045	0.017	0.055	0.001	0.002

Table 2. Non-linear parameters of the three hyperelastic models (mean ± standard deviation).

Pearson correlation coefficients (r)	Parameter A	Parameter D	Coefficient μ	Coefficient α	Constant C_1	Constant C_2
Control group–NaOH-treated group	–0.013	–0.344	–0.105	–0.578	0.163	–0.020

Table 3. Pearson correlation coefficients between the two groups.

Pearson correlation coefficients (r)	Parameters A and D	Coefficients μ and α	Constants C_1 and C_2
Control group	–0.932	–0.962	–0.987
NaOH-treated group	–0.967	–0.613	–0.976

Table 4. Pearson correlation coefficients between the model parameters of each hyperelastic model.

loss could be related to the disruption of lamella interweaving and collagen crosslinking^{19,23}. A negative correlation coefficient was observed for coefficients μ and α between the two sample groups, indicating the structural changes as well as the differences in structural behavior of the two groups.

The Mooney–Rivlin material constants C_1 and C_2 were obtained for the control and the NaOH-treated groups. The material constant C_1 was considerably different between the two groups ($p=0.001$). It was considerably decreased for the NaOH-treated samples possibly due to the structural damages within the tissue caused by the alkali solution. The material constant C_2 was significantly different for the two groups ($p=0.002$), while increased for the NaOH-treated samples compared to the control ones. This increase indicates a loss in the stiffness of the tissues which could be related to the structural disorganization in the collagen fibrils^{18–20,23}. A negative correlation coefficient was found for constant C_2 between the two sample groups.

The measurements of the parameters (A and D) involved in Hamilton–Zabolotskaya model represent the best fit explaining the statistical differences between the two groups ($p=0.0005$ and $p=0.0045$), respectively. The statistical significance of Mooney–Rivlin parameters (C_1 and C_2) is quantified determining the difference between the analyzed groups with p -values of $p=0.001$ and $p=0.002$, respectively, after applying an intermediate adjustment. Finally, the Ogden model has a low significant value in this study for the model parameters (μ and α) explaining the statistical differences between the two groups ($p=0.017$ and $p=0.055$), respectively.

In conclusion, quantification of non-linear model parameters of control and damaged corneal tissue is correlated to the changes in the tissue structure and its effect on the mechanical behavior of the cornea.

Received: 8 December 2019; Accepted: 23 June 2020

Published online: 14 July 2020

References

- Gonzalez-Andrades, M., Argüeso, P. & Gipson, I. Corneal anatomy. In *Corneal Regeneration—Therapy and Surgery* (ed. Alio, J.) (Springer, Berlin, 2019).
- Klintworth, G. K. Corneal dystrophies. *Orphanet. J. Rare Dis.* <https://doi.org/10.1186/1750-1172-4-7> (2009).
- Maharana, P. K. *et al.* Management of advanced corneal ectasias. *Br. J. Ophthalmol.* **100**(1), 34–40 (2016).
- Elham, R. *et al.* Keratoconus diagnosis using Corvis ST measured biomechanical parameters. *J. Curr. Ophthalmol.* **29**(3), 175–181 (2017).
- Kaushik, S. & Pandav, S. S. Ocular response analyzer. *J. Curr. Glaucoma Pract.* **6**(1), 17 (2012).
- Haustein, M., Spoerl, E. & Pillunat, L. Correlation of biomechanical parameters measured by corvis ST (Oculus) and by ocular response analyzer (ORA, Reichert). *Invest. Ophthalmol. Vis. Sci.* **54**(15), 1626–1626 (2013).
- Mikula, E., Hollman, K., Chai, D., Jester, J. V. & Juhasz, T. Measurement of corneal elasticity with an acoustic radiation force elasticity microscope. *Ultrasound Med Biol.* **40**(7), 1671–1679 (2014).
- Ogden, R. W. *Non-linear Elastic Deformations* (Courier Corporation, North Chelmsford, 1979).
- Rus, G. *et al.* Why are viscosity and nonlinearity bound to make an impact in clinical elastographic diagnosis?. *Sensors.* **20**(8), 2379 (2020).
- Ambekar, R., Toussaint, K. C. Jr. & Johnson, A. W. The effect of keratoconus on the structural, mechanical, and optical properties of the cornea. *J. Mech. Behav. Biomed.* **4**(3), 223–236 (2011).
- Nejad, T. M., Foster, C. & Gongal, D. Finite element modelling of cornea mechanics: A review. *Arq. Bras. Oftalmol.* **77**(1), 60–65 (2014).
- He, J. C., Marcos, S., Webb, R. H. & Burns, S. A. Measurement of the wave-front aberration of the eye by a fast psychophysical procedure. *JOSA A.* **15**(9), 2449–2456 (1998).
- Hatami-Marbini, H. & Jayaram, S. M. UVA/riboflavin collagen crosslinking stiffening effects on anterior and posterior corneal flaps. *Exp. Eye Res.* **176**, 53–58 (2018).
- Winkler, M. *et al.* Nonlinear optical macroscopic assessment of 3-D corneal collagen organization and axial biomechanics. *Invest. Ophthalm. Vis. Sci.* **52**(12), 8818–8827 (2011).
- Petsche, S. J., Chernyak, D., Martiz, J., Levenston, M. E. & Pinsky, P. M. Depth-dependent transverse shear properties of the human corneal stroma. *Invest Ophthalm. Vis. Sci.* **53**(2), 873–880 (2012).
- Dias, J., Diakonis, V. F., Kankariya, V. P., Yoo, S. H. & Ziebarth, N. M. Anterior and posterior corneal stroma elasticity after corneal collagen crosslinking treatment. *Exp. Eye Res.* **116**, 58–62 (2013).
- Mikula, E. R., Jester, J. V. & Juhasz, T. Measurement of an elasticity map in the human cornea. *Invest Ophthalm. Vis. Sci.* **57**(7), 3282–3286 (2016).
- Scarcelli, G., Besner, S., Pineda, R. & Yun, S. H. Biomechanical characterization of keratoconus corneas ex vivo with Brillouin microscopy. *Invest Ophthalm. Vis. Sci.* **55**(7), 4490–4495 (2014).
- Scarcelli, G., Besner, S., Pineda, R., Kalout, P. & Yun, S. H. In vivo biomechanical mapping of normal and keratoconus corneas. *Jama Ophthalmol.* **133**(4), 480–482 (2015).

20. Meek, K. M. *et al.* Changes in collagen orientation and distribution in keratoconus corneas. *Invest Ophthalm. Vis. Sci.* **46**(6), 1948–1956 (2005).
21. Morishige, N. *et al.* Second-harmonic imaging microscopy of normal human and keratoconus cornea. *Invest Ophthalm. Vis. Sci.* **48**(3), 1087–1094 (2007).
22. Morishige, N. *et al.* Quantitative analysis of collagen lamellae in the normal and keratoconic human cornea by second harmonic generation imaging microscopy. *Invest Ophthalm. Vis. Sci.* **55**(12), 8377–8385 (2014).
23. Mikula, E. *et al.* Axial mechanical and structural characterization of keratoconus corneas. *Exp. Eye Res.* **175**, 14–19 (2018).
24. Hamilton, M. F., Ilinskii, Y. A. & Zabolotskaya, E. A. Separation of compressibility and shear deformation in the elastic energy density (L). *J. Acoust. Soc. Am.* **116**(1), 41–44 (2004).
25. Landau, L. D. & Lifshitz, E. M. *Theoretical Physics, Theory of Elasticity* (Pergamon Press, Oxford, 1986).
26. Gilchrist, M.D., Destrade, M. *Third-And Fourth-Order Elasticity of Biological Soft Tissues*, 2010.
27. Ye, W., Bel-Brunon, A., Catheline, S., Combescur, A. & Rochette, M. Simulation of nonlinear transient elastography: Finite element model for the propagation of shear waves in homogeneous soft tissues. *Int. J. Numer. Meth. Biol.* **34**(1), e2901 (2018).
28. Alastrué, V., Calvo, B. & Doblaré, M. Biomechanical modeling of refractive corneal surgery. *J. Biomech. Eng.* **128**(1), 150–160 (2006).
29. Pandolfi, A. & Holzapfel, G. A. Three-dimensional modeling and computational analysis of the human cornea considering distributed collagen fibril orientations. *J. Biomech. Eng.* **130**(6), 061006 (2008).
30. Elsheikh, A. Finite element modeling of corneal biomechanical behavior. *J. Refract. Surg.* **26**(4), 289–300 (2010).
31. Nguyen, T. D. & Boyce, B. L. An inverse finite element method for determining the anisotropic properties of the cornea. *Biomech. Model Mech.* **10**(3), 323–337 (2011).
32. Su, P., Yang, Y. & Song, Y. Corneal hyper-viscoelastic model: derivations, experiments, and simulations. *Acta Bioeng. Biomech.* **17**, 2 (2015).
33. Whitford, C., Movchan, N. V., Studer, H. & Elsheikh, A. A viscoelastic anisotropic hyperelastic constitutive model of the human cornea. *Biomech. Model Mech.* **17**(1), 19–29 (2018).
34. Sharifi, R. *et al.* Finding an optimal corneal xenograft using comparative analysis of corneal matrix proteins across species. *Sci. Rep.* **9**(1), 1876 (2019).
35. Andrades, E. G. *et al.* Generación y caracterización de un modelo lesional corneal ex vivo para su uso en ingeniería tisular. *Actual Med.* **101**(797), 7–12 (2016).
36. Roberts, C. J. & Jun, L. (eds) *Corneal Biomechanics: From Theory to Practice* (Kugler Publications, Amsterdam, 2017).
37. Yazdi, A. A., Esteki, A., Dehghan, M. M. & Ghomsheh, F. T. The effect of displacement rate on viscoelastic properties of rat cervix. *Biomed. Eng. Appl. Bas. C.* **28**(03), 1650018 (2016).
38. Yazdi, A. A., Esteki, A., Dehghan, M. M. & Ghomsheh, F. T. Characterization of viscoelastic behavior of rat cervix in the last trimester of pregnancy. *Biomed Res.* **27**(4), 1194–1200 (2016).
39. Ashofteh Yazdi, A., Esteki, A. & Dehghan, M. M. Determination of an average quasi-linear viscoelastic model for the mechanical behavior of rat cervix. *P I Mech. Eng. L-J Mat.* **233**(5), 924–929 (2019).
40. Liu, T. *et al.* Characterization of hyperelastic mechanical properties for youth corneal anterior central stroma based on collagen fibril crimping constitutive model. *J. Mech. Behav. Biomed.* **103**, 103575 (2020).
41. Ogden, R. W. Large deformation isotropic elasticity—on the correlation of theory and experiment for incompressible rubberlike solids. *P. Roy. Soc. A-Math. Phys.* **326**(1567), 565–584 (1972).
42. Martins, P. A. L. S., Natal Jorge, R. M. & Ferreira, A. J. M. A comparative study of several material models for prediction of hyperelastic properties: Application to silicone-rubber and soft tissues. *Strain* **42**(3), 135–147 (2006).
43. Rus, G. *et al.* Mechanical biomarkers by torsional shear ultrasound for medical diagnosis. *J. Acoust. Soc. Am.* **144**(3), 1747–1747 (2018).
44. Melchor, J., Parnell, W. J., Bochud, N., Peralta, L. & Rus, G. Damage prediction via nonlinear ultrasound: A micro-mechanical approach. *Ultrasonics* **93**, 145–155 (2019).
45. Duck, F. A. Nonlinear acoustics in diagnostic ultrasound. *Ultrasonnd Med. Biol.* **28**(1), 1–18 (2002).
46. Bower, A. F. *Applied Mechanics of Solids* (CRC Press, Boca Raton, 2009).

Acknowledgements

This research was supported by the Ministry of Education, DPI2017-83859-R, DPI2014-51870-R, EQC2018-004508-P and UNGR15-CE-3664, Ministry of Health DTS15/00093, and Junta de Andalucía PI16/00339, PI-0107-2017, and PIN-0030-2017 projects. We thank Dr. Ionescu, Dr. Razvan, Prof. Cardona and Prof. Pérez Gómez at the Laboratory of Biomaterials Optics, Department of Optics, University of Granada (IBS. Granada), for their technical help taking representative images of the corneal samples used in this study.

Authors contribution

A.A.Y. and G.R. contributed in research design, data acquisition/research execution, data analysis and manuscript preparation. J.M. and M.G.A. contributed in research design, data analysis and manuscript preparation. J.T., I.F. and A.C. contributed in data acquisition/research execution. All the authors reviewed the manuscript.

Competing interests

The authors declare no competing interests.

Additional information

Correspondence and requests for materials should be addressed to M.G.-A. or G.R.

Reprints and permissions information is available at www.nature.com/reprints.

Publisher's note Springer Nature remains neutral with regard to jurisdictional claims in published maps and institutional affiliations.



Open Access This article is licensed under a Creative Commons Attribution 4.0 International License, which permits use, sharing, adaptation, distribution and reproduction in any medium or format, as long as you give appropriate credit to the original author(s) and the source, provide a link to the Creative Commons license, and indicate if changes were made. The images or other third party material in this article are included in the article's Creative Commons license, unless indicated otherwise in a credit line to the material. If material is not included in the article's Creative Commons license and your intended use is not permitted by statutory regulation or exceeds the permitted use, you will need to obtain permission directly from the copyright holder. To view a copy of this license, visit <http://creativecommons.org/licenses/by/4.0/>.

© The Author(s) 2020